2021 May

Antibody Display of cell surface receptor Tetraspanin12 and SARS-CoV-2 spike protein

Fu-Lien Hsieh[1,2,*], Tao-Hsin Chang[1,2,*]

[1]Department of Molecular Biology and Genetics

[2]Howard Hughes Medical Institute

Johns Hopkins University School of Medicine, Baltimore, MD 21205, United States.

[*]For correspondences: fulien.hsieh@gmail.com and taohsin.chang@gmail.com

Running Title: Tetraspanin12 and SARS-CoV-2 spike protein display on the antibody

Keywords: Antibody, display technology, Tetraspanin, SARS-CoV-2, retinal and infectious diseases

Number of pages: 34

Number of figures: 2

Number of tables: 0

Number of supplemental figures: 6

Number of supplemental tables: 0

Abstract

In previous work, Hsieh and Higgins presented a novel structure of antibodies identified from malaria-exposed individuals, in which the extracellular immunoglobulin (Ig)-like domain of leukocyte-associated immunoglobulin-like receptor 1 (LAIR1) is presented on the third complementarity determining regions (CDR3) of the Ig heavy chain. Here we develop an Antibody Display technology based on this LAIR1-containing antibody, by grafting proteins of interest (POI) onto the heavy chain CDR3 while retaining the biological properties of the POI. As a proof of principle, we displayed the second extracellular domain of Tetraspanin12 ($Tspan12_{EC2}$) and the receptor-binding domain (RBD) of SARS-CoV-2 spike protein on the heavy chain CDR3. Our data revealed that Antibody Display $Tspan12_{EC2}$ bound to Norrie Disease Protein (Norrin) and Antibody Display SARS-CoV-2 RBD bound to angiotensin-converting enzyme 2 (ACE2) and neutralizing nanobodies. Collectively, Antibody Display technology offers the general strategy of designing novel antibodies by grafting POI onto the CDR3.

Introduction

Antibodies are crucial reagents for biomedical research, diagnostics, and therapeutics. The conventional antibody, immunoglobulin G (IgG), has a highly conserved architecture that is composed of two heavy chains and two light chains (Owen et al., 2013). Each chain contains three hypervariable loops, known as complementarity-determining regions (CDRs), that form the antigen-binding site, which determines the binding specificity for antigens (Chothia et al., 1989). Unexpectedly, a group of unusual antibodies were identified recently from malaria-endemic regions of Africa (Tan et al., 2016). These antibodies have a remarkable feature of the antigen-binding site in which an intact collagen-binding domain, adopting the immunoglobulin (Ig)-like fold, from leukocyte-associated immunoglobulin-like receptor 1 (LAIR1) was inserted into the CDR3 of the heavy chain (**Figure 1A**). The LAIR1 insert carrying multiple somatic mutations interacts with the repetitive interspersed families of polypeptides (RIFIN) that are expressed on the surface of *Plasmodium falciparum*-infected erythrocytes (Tan et al., 2016). A detailed structural analysis of this LAIR1-containing antibody (MGD21) has been reported (Hsieh and Higgins, 2017). Pieper et al., further found that malaria-exposed individuals had two additional types of LAIR1-containing antibodies in which the LAIR1 insert was located between the variable domain of the heavy chain (V_H) and the constant domain of the heavy chain (C_{H1}) or fused to the FC fragment (Pieper et al., 2017).

The Tetraspanin (Tspan) receptor family contains 33 members in humans and play central roles in diverse biological processes (cell-cell fusion, immune response, and vascularization) and diseases (pathogen infection and tumorigenesis) (Charrin et al., 2014; Hemler, 2014; Vences-

Catalan and Levy, 2018). Previous structural analyses revealed that Tspan receptors adopt a conserved architecture composed of four transmembrane helices (TM1–TM4), intracellular N- and C-termini, a first and smaller extracellular domain (EC1; 13-30 residues) between TM1 and TM2, and a second and larger extracellular domain (EC2; 70-130 residues) between TM3 and TM4 (Kitadokoro et al., 2001; Oosterheert et al., 2020; Umeda et al., 2020; Yang et al., 2020b; Zimmerman et al., 2016). Functional studies showed that EC2 of Tspan receptors is typically a critical domain for the interactions with partner proteins or pathogens on the cell surface (Green et al., 2011; Rajesh et al., 2012; Zhu et al., 2002). Tspan12 is important in central nervous system (CNS) blood vessel development and blood-brain/retina barrier formation (Junge et al., 2009; Lai et al., 2017; Wang et al., 2018; Zhang et al., 2018). Genetic studies revealed that (1) deficiency of Tspan12 results in familial exudative vitreoretinopathy (FEVR), a hereditary disorder charactered by abnormal development of the retinal vasculature, often leading to retinal detachment and vision loss (Junge et al., 2009; Nikopoulos et al., 2010; Poulter et al., 2010), and (2) Tspan12 is a co-activator of Norrie Disease Protein (also named Norrin) mediated β-catenin signaling (Junge et al., 2009; Luhmann et al., 2005; Stenman et al., 2008; Xu et al., 2004). Norrin, a secreted cystine-knot growth factor, activates β-catenin signaling by binding to the extracellular cystine-rich domain (CRD) of Frizzled4 (Fz4) and the N-terminal domains of low-density lipoprotein receptor-related protein 5/6 (Lrp5/6) (Chang et al., 2015; Ke et al., 2013; Smallwood et al., 2007; Xu et al., 2004). Deficiencies of Fz4 and Lrp5 also result in FEVR (Robitaille et al., 2002; Toomes et al., 2004). Recently, Lai et al. suggested that the EC2 of Tspan12 ($Tspan12_{EC2}$) is a critical region for Norrin binding (Lai et al., 2017). However, whether $Tspan12_{EC2}$ interacts with Norrin directly remains obscure because of the technical challenge of

obtaining recombinant Tspan12$_{EC2}$ without its conserved transmembrane helices (Junge et al., 2009; Lai et al., 2017).

The worldwide spread of coronavirus disease-2019 (COVID-19) causing by severe acute respiratory syndrome coronavirus 2 (SARS-CoV-2) has become a global pandemic (Zhou et al., 2020a; Zhu et al., 2020). The surface of the SARS-CoV-2 particle is decorated with the heavily glycosylated trimeric spike (S) protein protruding from the virus membrane envelope (Fung and Liu, 2019; Shang et al., 2020; Walls et al., 2020; Wang et al., 2020b; Watanabe et al., 2020; Wrapp et al., 2020b; Yao et al., 2020). Specifically, SARS-CoV-2 S protein contains the receptor-binding domain (RBD) which mediates the interaction with a virus entry receptor, angiotensin-converting enzyme 2 (ACE2). Therefore, SARS-CoV-2 S protein is an attractive target for therapeutic and vaccine development (Hoffmann et al., 2020; Walls et al., 2020; Zhou et al., 2020a; Zhou et al., 2020b). SARS-CoV-2 S protein is immunogenic and the major target of neutralizing antibodies from COVID-19 convalescent individuals (Barnes et al., 2020; Baum et al., 2020; Brouwer et al., 2020; Chi et al., 2020; Ju et al., 2020; Seydoux et al., 2020; Walls et al., 2020; Wang et al., 2020a; Wu et al., 2020b). Furthermore, Piccoli et al., showed that more than 90% of these neutralizing antibodies from COVID-19 convalescent plasma target the RBD of SARS-CoV-2 S protein for protective humoral responses (Piccoli et al., 2020). However, recent studies showed that mutations in the RBD present in the current circulating SARS-CoV-2 variants decrease the potency of neutralizing antibodies (Greaney et al., 2021; Starr et al., 2021; Weisblum et al., 2020). Therefore, understanding how the RBD of SARS-CoV-2 S protein responds to ACE2 and neutralizing antibodies is critical for ongoing vaccine development,

114 immunotherapy, and the assessment of the RBD mutations occurring in circulating SARS-CoV-2
115 stains.
116
117 In this report, we have developed an antibody-based display approach, termed Antibody Display,
118 by grafting proteins of interest (POI) onto the heavy chain CDR3 to generate biological active
119 and stably folded chimera antibodies. As a proof of principle, we used the structure-guided
120 protein design approach based on the structure of LAIR1-containing antibody (Hsieh and
121 Higgins, 2017) to display the EC2 of Tspan12 and the RBD of SARS-CoV-2 S protein as
122 insertions at the tip of the heavy chain CDR3. We showed that Antibody Display $Tspan12_{EC2}$
123 ($Tspan12_{EC2}$-AD) bound to Norrin and Antibody Display SARS-CoV-2 RBD (RBD-AD) bound
124 to ACE2 and two neutralizing nanobodies (VHH-72 and H11-D4). We also designed a
125 humanized and engineering variable domain of the heavy chain alone to display the RBD of
126 SARS-CoV-2 and confirmed its binding properties.
127
128
129
130
131
132
133
134
135
136

Result

Design, expression and purification of Antibody Display Tspan12$_{EC2}$

The design of the Antibody Display was informed by structural studies of LAIR1-containing antibody (**Figure 1A**) (Hsieh and Higgins, 2017). We hypothesized that POI could graft onto the heavy chain CDR3 via two short peptide linkers to generate chimeric antibodies while retaining the biological features of the POI. To test this concept, we focused initially on Tspan12$_{EC2}$, because (1) Tspan12$_{EC2}$ protrudes from two transmembrane helices of Tspan12 suggesting that the N- and C-termini of Tspan12$_{EC2}$ could be linked to β-strands G and F of the heavy chain in a manner that preserves their native spacing (**Figure 1B**) and (2) the biomedical importance of Tspan12 in retinal vascular diseases.

We began our design by searching for homologous structures and conducting a multiple sequence alignment of Tspan25 (CD53) (Yang et al., 2020b), Tspan28 (CD81) (Kitadokoro et al., 2001; Zimmerman et al., 2016), and Tspan29 (CD9) (Oosterheert et al., 2020; Umeda et al., 2020) with Tspan12, as shown in **Figure 1–Figure supplement 1A**. The obtained information led us to generate constructs having different boundaries of Tspan12$_{EC2}$ for expression trials in HEK293T cells (**Figure 1–Figure supplement 1B**). The constructs contained an N-terminal signal peptide and C-terminal monomeric Venus (mVenus) and 12xHis tags. To assess the level of secreted mVenus fusion protein expression, we used a time- and cost-efficient method, immobilized metal affinity chromatography (IMAC) followed by in-gel fluorescent imaging (Chang et al., 2020). Variations in the location of the Tspan12$_{EC2}$ N- and C-termini produced large effects on protein yield (**Figure 1–Figure supplement 1C**). Construct 4 (Tspan12 residues

116-220) exhibited the highest yield, somewhat less than 0.1 mg/L, consistent with previous studies showing the technical difficulties in producing recombinant Tspan12$_{EC2}$ (Junge et al., 2009; Lai et al., 2017). As the secretory pathway in mammalian cells has stringent protein quality-control machinery to ensure that secreted proteins are folded correctly (Trombetta and Parodi, 2003), the expression trials imply that residues 116-220 corresponds to a core folding unit of Tspan12$_{EC2}$.

We next generated a three-dimensional model of Tspan12$_{EC2}$ and designed Antibody Display Tspan12$_{EC2}$ (Tspan12$_{EC2}$-AD) model in a Fab format, Fab (Tspan12$_{EC2}$), by computationally grafting the Tspan12$_{EC2}$ onto the heavy chain CDR3 based on the structure of LAIR1-containing antibody (**Figure 1C**). We designed constructs based on these principles: (1) placing the core folding unit of Tspan12$_{EC2}$ at the tip of the heavy chain CDR3 to maximally expose its binding regions for ligand binding, (2) preventing steric clashes between the Tspan12$_{EC2}$ and the CDR loops of the heavy chain and light chain, and (3) testing variations in the length and flexibility of the connecting linkers between the Tspan12$_{EC2}$ and the heavy chain. Five designs of these chimeric heavy chain constructs (**Figure 1–Figure supplement 2A**) were co-transfected with light chain constructs in HEK293T cells to yield secreted Fab proteins and were assessed for expression level using IMAC followed by in-gel fluorescent imaging (**Figure 1–Figure supplement 2B**). Interestingly, only two of these designs (construct 1 and 5) could be expressed as secreted Fab proteins by passing the protein quality-control machinery in mammalian cells (**Figure 1–Figure supplement 2B**). Specifically, Tspan12$_{EC2}$-AD (construct 5) with the highest yield contained Tspan12 residues 115-220 and had the shortest connecting linkers (**Figure 1–Figure supplement 2B**). This Tspan12$_{EC2}$-AD was produced at 1 mg/L, a yield close to that of

183 the LAIR1-containing antibody (Hsieh and Higgins, 2017), and showed a 10-fold higher
184 expression level than Tspan12$_{EC2}$ (**Figure 1–Figure supplement 1C**).
185
186 **Functional analyses of Antibody Display Tspan12$_{EC2}$**
187 Next, to assess if Tspan12$_{EC2}$-AD adopted the correct fold of Tspan12$_{EC2}$, we tested the ability of
188 recombinant Tspan12$_{EC2}$ to bind to Norrin as measured by a colorimetric alkaline phosphatase
189 (AP) reaction-based protein-protein interaction assay using an AP-Norrin fusion protein as a
190 probe (Xu et al., 2004). Each bait protein had a biotinylated C-terminal Avi-tag and was captured
191 on a streptavidin coated micro-well. Tspan12$_{EC2}$ bound to AP-Norrin (**Figure 1D** and **Figure 1–**
192 **Figure supplement 3**), as did the CRD of Fz4 (Fz4$_{CRD}$) and the leucine-rich repeat domain of
193 Leucine-rich repeat containing G-protein coupled receptor 4 (Lgr4$_{LRR}$), extracellular domains
194 that are known to bind to Norrin (Chang et al., 2015; Deng et al., 2013; Shen et al., 2015; Xu et
195 al., 2004). As expected, AP-Norrin did not bind to Fz5$_{CRD}$ (**Figure 1D**) (Chang et al., 2015;
196 Smallwood et al., 2007). Importantly, Tspan12$_{EC2}$-AD bound to AP-Norrin as did Tspan12$_{EC2}$
197 (**Figure 1D**). Taken together, these results show that (1) EC2 of Tspan12 mediates Norrin
198 binding, in agreement with previous genetic studies using domain swaps within full-length
199 Tspan12 together with co-immunoprecipitation (Lai et al., 2017), and (2) correctly folded
200 Tspan12$_{EC2}$ can be grafted onto the heavy chain CDR3 without losing Norrin binding.
201
202 **Design, expression and purification of Antibody Display SARS-CoV-2 RBD**
203 To assess whether the design principle of the Antibody Display can apply to other protein folds,
204 we tested the RBD of SARS-CoV-2 S protein. We began the design of the Antibody Display
205 SARS-CoV-2 RBD (RBD-AD) by searching the three-dimensional RBD structures of SARS-

CoV-2 S protein (Barnes et al., 2020; Huo et al., 2020; Lan et al., 2020; Shang et al., 2020; Walls et al., 2020; Wang et al., 2020b; Wrapp et al., 2020b; Yuan et al., 2020; Zhou et al., 2020b). As shown in **Figure 2A**, we computationally grafted the RBD structure of SARS-CoV-2 S protein onto the heavy chain CDR3 of LAIR1-containing antibody to generate a model in in a Fab format, Fab (RBD), by using the same design principles as Tspan12$_{EC2}$-AD.

Furthermore, we hypothesized that a single V_H domain could serve as a scaffold to display SARS-CoV-2 RBD in the absence of light chains. Indeed, human single V_H domain mimicking nanobodies from camels has been developed as a minimum size of antigen recognition unit in the absence of light chains (Davies and Riechmann, 1995; Hamers-Casterman et al., 1993), although specific hallmark mutations are required to maintain the solubility and the binding property of the single V_H domain (Davies and Riechmann, 1995; Hamers-Casterman et al., 1993; Muyldermans, 2013). More recently, Wu et al., identified a highly soluble and stable single V_H domain from the human germline Ig heavy chain variable region 3-66*1 (IGHV3-66*1) allele (Wu et al., 2020a). Therefore, we next designed an engineered single V_H domain (eV_H) based on the IGHV3-66*1 for the display of SARS-CoV-2 RBD, eV_H(RBD), as shown in **Figure 2–Figure supplement 2**.

Functional analyses of Antibody Display SARS-CoV-2 RBD

To verify whether RBD-AD retained binding to ACE2 and neutralizing antibodies, we generated AP fusion proteins with the extracellular domain of ACE2 (ACE2$_{ECD}$-AP) and two anti-RBD nanobodies (NB$_{VHH-72}$-AP and NB$_{H11-D4}$-AP) (Huo et al., 2020; Wrapp et al., 2020a) (**Figure 2–Figure supplement 2**). We next prepared bait proteins of RBD-AD: (1) Fab (RBD) and

229 eV_H(RBD) constructs had a C-terminal mVenus and biotinylated Avi-tag, immobilized on
230 streptavidin-coated wells (**Figure 2B** and **Figure 2–Figure supplement 3**), and (2) an
231 eV_H(RBD) construct contained the human IgG Fc fusion at the C-terminus, immobilized on a
232 protein G-coated well (**Figure 2C**). As measured the binding by AP reaction-based assays, Fab
233 (RBD) and eV_H(RBD) bound robustly and specifically to $ACE2_{ECD}$-AP, $NB_{VHH\text{-}72}$-AP, and
234 $NB_{H11\text{-}D4}$-AP (**Figure 2B-C** and **Figure 2–Figure supplement 3**). We conclude that RBD of
235 SARS-CoV-2 S protein can be displayed on the heavy chain CDR3 in functional form.
236
237
238
239
240
241
242
243
244
245
246
247
248
249
250
251

Discussion

We present a novel antibody engineering approach, named Antibody Display, by grafting POI onto the heavy chain CDR3, which were designed through a structure-guided approach built on the architecture of LAIR1-containing antibodies naturally occurred in malaria-exposed individuals (Hsieh and Higgins, 2017; Tan et al., 2016). Most importantly, each POI retained its biological properties by taking advantage of the structural conservation and stability of the antibody Ig fold. As a proof of principle, we showed that the design and production of Tspan12$_{EC2}$-AD and RBD-AD were successful. Colorimetric AP reaction-based binding assays further revealed that Tspan12$_{EC2}$-AD bound to Norrin and RBD-AD bound to ACE2 and NBs (VHH-72 and H11-D4). Our findings suggest a generic design principle of the Antibody Display, particularly for the POI adopting a non-Ig like fold: (1) a known structure or a computational model derived from homologous protein structures, (2) N and C termini in proximity to graft onto the β-strands G and F of the heavy chain, and (3) prevention of steric clashes with the antibody. At present, the limitations for selecting POI for Antibody Display such as protein shape and size remain unclear; further studies will be required to address these questions.

Comparing with conventional Fc fusion proteins in which the POI is fused to the N terminus of Fc usually including the flexible hinge region, we reasoned that the Antibody Display, which grafts the POI onto the β-strands G and F of the heavy chain, provides several potential advantages: (1) design and production of a more conformationally constrained chimeric protein, (2) reduction of proteolysis with the POI inserted into a stable antibody Ig fold, and (3) extension

of the current antibody engineering toolkit for generating bispecific and chimeric antibodies. Further studies will be needed to explore these potential advantages.

An intriguing feature of using the Antibody Display for Tspan12$_{EC2}$ is with a better yield of protein production than Tspan12$_{EC2}$. Our functional assays demonstrated that Tspan12$_{EC2}$ bound to Norrin directly, in agreement with previous genetic studies (Lai et al., 2017). As Tspan12 playing critical roles in CNS vascular development (Junge et al., 2009; Zhang et al., 2018) and tumorigenesis (Knoblich et al., 2014; Otomo et al., 2014), Tspan12$_{EC2}$-AD may be a useful reagent for these studies. Moreover, Tspan proteins are well known for their important roles in regulating tumor migration, invasion and metastasis (Charrin et al., 2014; Hemler, 2014; Vences-Catalan and Levy, 2018). Antibodies targeting Tspan29 (CD9), particularly on its EC2 region, have been shown to inhibit the progression of colorectal and gastric cancers (Nakamoto et al., 2009; Ovalle et al., 2007). Furthermore, Tspan proteins are used by several pathogens for infection (Charrin et al., 2014). For example, Hepatitis C Virus and *P. falciparum* use Tspan28 (CD81) for infection of hepatocytes (Pileri et al., 1998; Silvie et al., 2003). However, research on Tspan receptors has been hampered by the lack of an efficient approach to produce recombinant EC2 proteins. So far, only Tspan25 (CD53), Tspan28 (CD81), and Tspan29 (CD9) have been produced for biochemical and structural analyses among 33 Tspan receptors (Kitadokoro et al., 2001; Oosterheert et al., 2020; Umeda et al., 2020; Yang et al., 2020b; Zimmerman et al., 2016). More studies will be required to investigate whether the Antibody Display can apply to other Tspan proteins.

SARS-CoV-2 has resulted in a global pandemic and several types of COVID-19 vaccines such as nucleic acids, viral vectors, and protein subunits have been developed for vaccinations globally (Connors et al., 2021). Ongoing studies have shown that the RBD of SARS-CoV-2 S protein is the major target of neutralizing antibodies from COVID-19 convalescent individuals (Barnes et al., 2020; Baum et al., 2020; Brouwer et al., 2020; Chi et al., 2020; Ju et al., 2020; Piccoli et al., 2020; Seydoux et al., 2020; Walls et al., 2020; Wang et al., 2020a; Wu et al., 2020b), consistent with recent findings showing that the RBD, particularly decorated on nanoparticles, can induce a protective humoral immune response against SARS-CoV-2 infection (Cohen et al., 2021; Tan et al., 2021; Yang et al., 2020a). In this report, we demonstrated that the Antibody Display can be used to display the RBD of SARS-CoV-2 S protein on the heavy chain CDR3 without losing its binding properties. It is not yet known whether RBD-AD can induce neutralizing antibodies, but it would be an interesting test case and it could be relevant for the future preparedness and response capacity against emerging SARS-CoV-2 variants.

Materials and Methods

Construct design and molecular cloning

The human complementary DNA clones of Fz4, Fz5, and Tspan12 were gifts from Jeremy Nathans and the human ACE2 clone (Shang et al., 2020) was obtained from Addgene (code 145033). Synthetic DNA fragments of engineered V_H containing SARS-CoV-2 RBD (resi 333-527; with a P527A mutation; UniProtKB code P0DTC2; **Figure 2–Figure supplement 2**), $NB_{VHH\text{-}72}$ (PDB code 6WAQ), and $NB_{H11\text{-}D4}$ (PDB code 6YZ5) were obtained from Integrated DNA Technologies. Expression plasmids of MGD21 heavy chain pOPINVH and MGD21 light chain pOPINVL were described Hsieh and Higgins, 2017. The AP fusion Norrin construct was described in Xu et al., 2004.

The following five backbone constructs used for the Fc fusion or biotinylated baits and AP fusion probes were derived from the pHLsec vector (Aricescu et al., 2006). (1) The pHLsec-3C-Fc (C103A)-8H vector contains a C-terminal Human Rhinovirus (HRV)-3C protease cleavage site followed by the human immunoglobulin heavy constant gamma 1 (resi 102-330; having a C103A mutation to remove an unpaired cysteine; UniProtKB code P01857) and an 8xHis tag. (2) The pHLsec-Fc-Avi-6H vector contains the human immunoglobulin heavy constant gamma 1 (resi 101-330; UniProtKB code P01857) followed by an Avi tag that can be biotinylated by BirA ligases and a 6xHis tag. (3) The pHLsec-3C-mVenus-Avi-8H vector derived from pHLsec-mVenus-12H (Chang et al., 2015) was tagged with a C-terminally HRV-3C protease cleavage site followed by a mVenus fusion protein, an Avi tag and finally an 8xHis tag. (4) The pHL-N-AP-Myc-8H vector was constructed N-terminally with the human alkaline phosphatase (AP; resi

1-506; NCBI code NP_001623) followed by a Myc tag and finally a C-terminal 8xHis tag. (5) The pHLsec-C-Myc-AP-8H vector contains a C-terminal Myc tag followed by the human AP (resi 18-506; NCBI code NP_001623) and finally an 8xHis tag.

Tspan12 coding segments for the EC2 were PCR-amplified and cloned into the pHLsec-mVenus-12H (Chang et al., 2020; Chang et al., 2015). $Tspan12_{EC2}$ inserts were grafted into a modified MGD21 heavy chain vector containing a C-terminal HRV-3C protease cleavage site followed by a mVenus fusion protein and finally an 8xHis tag (pHLsec-mMGD21-3C-mVenus-Avi-8H), by using three-fragments overlapping PCR experiments. The MGD21 light chain mutant (C91A and C93A) vector was generated by using a two-step overlapping PCR method. A DNA segment coding for CRD of Fz4 (resi 40-179) was constructed into the pHLsec-Fc-Avi-6H and pHLsec-3C-mVenus-Avi-8H. The CRD of Fz5 (resi 31-181) were cloned into the pHLsec-Fc-Avi-6H, pHLsec-3C-mVenus-Avi-8H, and pHL-N-AP-Myc-8H vectors. The $Lgr4_{LRR}$ was constructed into the pHLsec-3C-mVenus-Avi-8H vector. SARS-CoV-2 RBD insert was grafted into the pHLsec-mMGD21-3C-mVenus-Avi-8H vector. An engineered V_H containing SARS-CoV-2 RBD was constructed into the pHLsec-3C-mVenus-Avi-8H and pHLsec-3C-Fc (C103A)-8H vectors. $ACE2_{ECD}$ (resi 19-615), NB_{VHH-72}, and NB_{H11-D4} were cloned into the pHLsec-AP-8H vector. All constructs were confirmed by sequencing.

Computational modeling and structure-based design

The HHpred server (Soding et al., 2005; Zimmermann et al., 2018) was used to search for homologs of $Tspan12_{EC2}$ in the protein structure database of the Protein Data Bank (PDB). The structures of Tspan28 (CD81; PDB codes 1G8Q and 5TCX) were selected to generate an initial

365 computational model of Tspan12$_{EC2}$ with Modeller (Eswar et al., 2006). Notably, the structures
366 of Tspan25 (CD53; PDB code 6WVG), and Tspan29 (CD9, PDB codes 6RLR and 6K4J) were
367 not available during the HHpred search. For the protein design of Antibody Display Tspan12$_{EC2}$,
368 LAIR1 insert was removed from the model of MGD21 Fab fragment (PDB code 5NST) and the
369 Tspan12$_{EC2}$ model was docked into the MGD21 V_H manually by using COOT (Emsley et al.,
370 2010) and PyMOL Molecular Graphic System (Schrödinger, LLC). For the structure-guided
371 design of Antibody Display SARS-CoV-2 RBD, the crystal structure of SARS-CoV-2 RBD
372 (PBD code 6YLA) was selected and docked into the V_H region of the antibody manually by
373 using COOT (Emsley et al., 2010).
374
375 **Protein expression and purification**
376 HEK293T (ATCC CRL-11268) cells were maintained and transfected with the DNA using
377 polyethylenimine (MilliporeSigma 408727) following the established procedures (Aricescu et
378 al., 2006; Chang et al., 2015; Hsieh and Higgins, 2017; Hsieh et al., 2016). For Antibody Display
379 Tspan12$_{EC2}$, DNA constructs expressing heavy chain and light chain were mixed into a 1 to 1
380 ratio and co-expressed in HEK293T cells. For the biotinylated bait preparations, bait constructs
381 were mixed with a pHLsec-BirA-ER vector (Chang et al., 2015) into a 3 to 1 ratio and co-
382 transfected in HEK293T cells in the presence of 0.1 mM Biotin (MilliporeSigma B4639). The
383 biotinylated baits were purified from conditioned media by the immobilized metal affinity
384 chromatography (IMAC) method as previously described in (Chang et al., 2020). IMAC method
385 was also used for the purification of His tagged Fc fusion and AP fusion proteins. To evaluate
386 the expression level of secreted mVenus fusion proteins from conditioned media, IMAC

387 followed by an in-gel fluorescence imaging method was used as previously described in (Chang
388 et al., 2020).
389
390 **Alkaline Phosphatase based binding assay**
391 The purified Fc fusion baits were captured on 96-well protein-G coated plates (Thermo Fisher
392 Scientific 15131). The biotinylated baits were immobilized on 96-well streptavidin-coated plates
393 (Thermo Fisher Scientific 15500). The wells were then washed three times with wash buffer (10
394 mM HEPES, pH 7.5, 0.15 M NaCl, 0.05% (w/v) Tween-20) and incubated with a 10-fold
395 dilution of Blocker bovine serum albumin (BSA; Thermo Fisher Scientific 37525) in wash buffer
396 for 1 h at 25 °C. The wells were washed with wash buffer and incubated with conditioned media
397 containing AP probes at 4 °C overnight. The wells were subsequently washed three times with
398 wash buffer and incubated with BluePhos phosphatase substrate solution (Kirkegaard and Perry
399 Laboratories 50-88-00) to visualize the bound AP probes.
400
401
402
403
404
405
406
407
408
409

Acknowledgements

We thank Jeremy Nathans for access to the laboratory and valuable comments on the manuscript; and Matthew Higgins for critical reading the manuscript and valuable comments. F-L H was supported by the Howard Hughes Medical Institute. T-H C was supported by a Human Frontier Science Program long-term fellowship (LT000130/2017-L).

Contributions

F-L H and T-H C conceived the project, conducted experiments, and wrote the manuscript.

Competing Interests

F-L H and T-H C declare no competing interests.

421

References

Aricescu, A.R., Lu, W., and Jones, E.Y. (2006). A time- and cost-efficient system for high-level protein production in mammalian cells. Acta Crystallogr D Biol Crystallogr *62*, 1243-1250.
Barnes, C.O., West, A.P., Jr., Huey-Tubman, K.E., Hoffmann, M.A.G., Sharaf, N.G., Hoffman, P.R., Koranda, N., Gristick, H.B., Gaebler, C., Muecksch, F.*, et al.* (2020). Structures of Human Antibodies Bound to SARS-CoV-2 Spike Reveal Common Epitopes and Recurrent Features of Antibodies. Cell *182*, 828-842 e816.
Baum, A., Fulton, B.O., Wloga, E., Copin, R., Pascal, K.E., Russo, V., Giordano, S., Lanza, K., Negron, N., Ni, M.*, et al.* (2020). Antibody cocktail to SARS-CoV-2 spike protein prevents rapid mutational escape seen with individual antibodies. Science *369*, 1014-1018.
Brouwer, P.J.M., Caniels, T.G., van der Straten, K., Snitselaar, J.L., Aldon, Y., Bangaru, S., Torres, J.L., Okba, N.M.A., Claireaux, M., Kerster, G.*, et al.* (2020). Potent neutralizing antibodies from COVID-19 patients define multiple targets of vulnerability. Science *369*, 643-650.
Chang, T.H., Hsieh, F.L., Smallwood, P.M., Gabelli, S.B., and Nathans, J. (2020). Structure of the RECK CC domain, an evolutionary anomaly. Proc Natl Acad Sci U S A *117*, 15104-15111.
Chang, T.H., Hsieh, F.L., Zebisch, M., Harlos, K., Elegheert, J., and Jones, E.Y. (2015). Structure and functional properties of Norrin mimic Wnt for signalling with Frizzled4, Lrp5/6, and proteoglycan. Elife *4*.
Charrin, S., Jouannet, S., Boucheix, C., and Rubinstein, E. (2014). Tetraspanins at a glance. J Cell Sci *127*, 3641-3648.
Chi, X., Yan, R., Zhang, J., Zhang, G., Zhang, Y., Hao, M., Zhang, Z., Fan, P., Dong, Y., Yang, Y.*, et al.* (2020). A neutralizing human antibody binds to the N-terminal domain of the Spike protein of SARS-CoV-2. Science *369*, 650-655.
Chothia, C., Lesk, A.M., Tramontano, A., Levitt, M., Smith-Gill, S.J., Air, G., Sheriff, S., Padlan, E.A., Davies, D., Tulip, W.R.*, et al.* (1989). Conformations of immunoglobulin hypervariable regions. Nature *342*, 877-883.
Cohen, A.A., Gnanapragasam, P.N.P., Lee, Y.E., Hoffman, P.R., Ou, S., Kakutani, L.M., Keeffe, J.R., Wu, H.J., Howarth, M., West, A.P.*, et al.* (2021). Mosaic nanoparticles elicit cross-reactive immune responses to zoonotic coronaviruses in mice. Science.
Connors, M., Graham, B.S., Lane, H.C., and Fauci, A.S. (2021). SARS-CoV-2 Vaccines: Much Accomplished, Much to Learn. Ann Intern Med.
Davies, J., and Riechmann, L. (1995). Antibody VH domains as small recognition units. Biotechnology (N Y) *13*, 475-479.
Deng, C., Reddy, P., Cheng, Y., Luo, C.W., Hsiao, C.L., and Hsueh, A.J. (2013). Multi-functional norrin is a ligand for the LGR4 receptor. J Cell Sci *126*, 2060-2068.
Fung, T.S., and Liu, D.X. (2019). Human Coronavirus: Host-Pathogen Interaction. Annu Rev Microbiol *73*, 529-557.
Greaney, A.J., Starr, T.N., Gilchuk, P., Zost, S.J., Binshtein, E., Loes, A.N., Hilton, S.K., Huddleston, J., Eguia, R., Crawford, K.H.D.*, et al.* (2021). Complete Mapping of Mutations to the SARS-CoV-2 Spike Receptor-Binding Domain that Escape Antibody Recognition. Cell Host Microbe *29*, 44-57 e49.

Green, L.R., Monk, P.N., Partridge, L.J., Morris, P., Gorringe, A.R., and Read, R.C. (2011). Cooperative role for tetraspanins in adhesin-mediated attachment of bacterial species to human epithelial cells. Infect Immun *79*, 2241-2249.
Hamers-Casterman, C., Atarhouch, T., Muyldermans, S., Robinson, G., Hamers, C., Songa, E.B., Bendahman, N., and Hamers, R. (1993). Naturally occurring antibodies devoid of light chains. Nature *363*, 446-448.
Hemler, M.E. (2014). Tetraspanin proteins promote multiple cancer stages. Nat Rev Cancer *14*, 49-60.
Hoffmann, M., Kleine-Weber, H., Schroeder, S., Kruger, N., Herrler, T., Erichsen, S., Schiergens, T.S., Herrler, G., Wu, N.H., Nitsche, A.*, et al.* (2020). SARS-CoV-2 Cell Entry Depends on ACE2 and TMPRSS2 and Is Blocked by a Clinically Proven Protease Inhibitor. Cell *181*, 271-280 e278.
Hsieh, F.L., and Higgins, M.K. (2017). The structure of a LAIR1-containing human antibody reveals a novel mechanism of antigen recognition. Elife *6*.
Hsieh, F.L., Turner, L., Bolla, J.R., Robinson, C.V., Lavstsen, T., and Higgins, M.K. (2016). The structural basis for CD36 binding by the malaria parasite. Nat Commun *7*, 12837.
Huo, J., Zhao, Y., Ren, J., Zhou, D., Duyvesteyn, H.M.E., Ginn, H.M., Carrique, L., Malinauskas, T., Ruza, R.R., Shah, P.N.M.*, et al.* (2020). Neutralization of SARS-CoV-2 by Destruction of the Prefusion Spike. Cell Host Microbe *28*, 445-454 e446.
Ju, B., Zhang, Q., Ge, J., Wang, R., Sun, J., Ge, X., Yu, J., Shan, S., Zhou, B., Song, S.*, et al.* (2020). Human neutralizing antibodies elicited by SARS-CoV-2 infection. Nature *584*, 115-119.
Junge, H.J., Yang, S., Burton, J.B., Paes, K., Shu, X., French, D.M., Costa, M., Rice, D.S., and Ye, W. (2009). TSPAN12 regulates retinal vascular development by promoting Norrin- but not Wnt-induced FZD4/beta-catenin signaling. Cell *139*, 299-311.
Ke, J., Harikumar, K.G., Erice, C., Chen, C., Gu, X., Wang, L., Parker, N., Cheng, Z., Xu, W., Williams, B.O.*, et al.* (2013). Structure and function of Norrin in assembly and activation of a Frizzled 4-Lrp5/6 complex. Genes Dev *27*, 2305-2319.
Kitadokoro, K., Bordo, D., Galli, G., Petracca, R., Falugi, F., Abrignani, S., Grandi, G., and Bolognesi, M. (2001). CD81 extracellular domain 3D structure: insight into the tetraspanin superfamily structural motifs. EMBO J *20*, 12-18.
Knoblich, K., Wang, H.X., Sharma, C., Fletcher, A.L., Turley, S.J., and Hemler, M.E. (2014). Tetraspanin TSPAN12 regulates tumor growth and metastasis and inhibits beta-catenin degradation. Cell Mol Life Sci *71*, 1305-1314.
Lai, M.B., Zhang, C., Shi, J., Johnson, V., Khandan, L., McVey, J., Klymkowsky, M.W., Chen, Z., and Junge, H.J. (2017). TSPAN12 Is a Norrin Co-receptor that Amplifies Frizzled4 Ligand Selectivity and Signaling. Cell Rep *19*, 2809-2822.
Lan, J., Ge, J., Yu, J., Shan, S., Zhou, H., Fan, S., Zhang, Q., Shi, X., Wang, Q., Zhang, L.*, et al.* (2020). Structure of the SARS-CoV-2 spike receptor-binding domain bound to the ACE2 receptor. Nature *581*, 215-220.
Luhmann, U.F., Lin, J., Acar, N., Lammel, S., Feil, S., Grimm, C., Seeliger, M.W., Hammes, H.P., and Berger, W. (2005). Role of the Norrie disease pseudoglioma gene in sprouting angiogenesis during development of the retinal vasculature. Invest Ophthalmol Vis Sci *46*, 3372-3382.
Muyldermans, S. (2013). Nanobodies: natural single-domain antibodies. Annu Rev Biochem *82*, 775-797.

Nakamoto, T., Murayama, Y., Oritani, K., Boucheix, C., Rubinstein, E., Nishida, M., Katsube, F., Watabe, K., Kiso, S., Tsutsui, S.*, et al.* (2009). A novel therapeutic strategy with anti-CD9 antibody in gastric cancers. J Gastroenterol *44*, 889-896.
Nikopoulos, K., Gilissen, C., Hoischen, A., van Nouhuys, C.E., Boonstra, F.N., Blokland, E.A., Arts, P., Wieskamp, N., Strom, T.M., Ayuso, C.*, et al.* (2010). Next-generation sequencing of a 40 Mb linkage interval reveals TSPAN12 mutations in patients with familial exudative vitreoretinopathy. Am J Hum Genet *86*, 240-247.
Oosterheert, W., Xenaki, K.T., Neviani, V., Pos, W., Doulkeridou, S., Manshande, J., Pearce, N.M., Kroon-Batenburg, L.M., Lutz, M., van Bergen En Henegouwen, P.M.*, et al.* (2020). Implications for tetraspanin-enriched microdomain assembly based on structures of CD9 with EWI-F. Life Sci Alliance *3*.
Otomo, R., Otsubo, C., Matsushima-Hibiya, Y., Miyazaki, M., Tashiro, F., Ichikawa, H., Kohno, T., Ochiya, T., Yokota, J., Nakagama, H.*, et al.* (2014). TSPAN12 is a critical factor for cancer-fibroblast cell contact-mediated cancer invasion. Proc Natl Acad Sci U S A *111*, 18691-18696.
Ovalle, S., Gutierrez-Lopez, M.D., Olmo, N., Turnay, J., Lizarbe, M.A., Majano, P., Molina-Jimenez, F., Lopez-Cabrera, M., Yanez-Mo, M., Sanchez-Madrid, F.*, et al.* (2007). The tetraspanin CD9 inhibits the proliferation and tumorigenicity of human colon carcinoma cells. Int J Cancer *121*, 2140-2152.
Owen, J.A., Punt, J., Stranford, S.A., Jones, P.P., and Kuby, J. (2013). Kuby immunology, 7th edn (New York: W.H. Freeman).
Piccoli, L., Park, Y.J., Tortorici, M.A., Czudnochowski, N., Walls, A.C., Beltramello, M., Silacci-Fregni, C., Pinto, D., Rosen, L.E., Bowen, J.E.*, et al.* (2020). Mapping Neutralizing and Immunodominant Sites on the SARS-CoV-2 Spike Receptor-Binding Domain by Structure-Guided High-Resolution Serology. Cell *183*, 1024-1042 e1021.
Pieper, K., Tan, J., Piccoli, L., Foglierini, M., Barbieri, S., Chen, Y., Silacci-Fregni, C., Wolf, T., Jarrossay, D., Anderle, M.*, et al.* (2017). Public antibodies to malaria antigens generated by two LAIR1 insertion modalities. Nature *548*, 597-601.
Pileri, P., Uematsu, Y., Campagnoli, S., Galli, G., Falugi, F., Petracca, R., Weiner, A.J., Houghton, M., Rosa, D., Grandi, G.*, et al.* (1998). Binding of hepatitis C virus to CD81. Science *282*, 938-941.
Poulter, J.A., Ali, M., Gilmour, D.F., Rice, A., Kondo, H., Hayashi, K., Mackey, D.A., Kearns, L.S., Ruddle, J.B., Craig, J.E.*, et al.* (2010). Mutations in TSPAN12 cause autosomal-dominant familial exudative vitreoretinopathy. Am J Hum Genet *86*, 248-253.
Rajesh, S., Sridhar, P., Tews, B.A., Feneant, L., Cocquerel, L., Ward, D.G., Berditchevski, F., and Overduin, M. (2012). Structural basis of ligand interactions of the large extracellular domain of tetraspanin CD81. J Virol *86*, 9606-9616.
Robitaille, J., MacDonald, M.L., Kaykas, A., Sheldahl, L.C., Zeisler, J., Dube, M.P., Zhang, L.H., Singaraja, R.R., Guernsey, D.L., Zheng, B.*, et al.* (2002). Mutant frizzled-4 disrupts retinal angiogenesis in familial exudative vitreoretinopathy. Nat Genet *32*, 326-330.
Seydoux, E., Homad, L.J., MacCamy, A.J., Parks, K.R., Hurlburt, N.K., Jennewein, M.F., Akins, N.R., Stuart, A.B., Wan, Y.H., Feng, J.*, et al.* (2020). Analysis of a SARS-CoV-2-Infected Individual Reveals Development of Potent Neutralizing Antibodies with Limited Somatic Mutation. Immunity *53*, 98-105 e105.
Shang, J., Ye, G., Shi, K., Wan, Y., Luo, C., Aihara, H., Geng, Q., Auerbach, A., and Li, F. (2020). Structural basis of receptor recognition by SARS-CoV-2. Nature *581*, 221-224.

Shen, G., Ke, J., Wang, Z., Cheng, Z., Gu, X., Wei, Y., Melcher, K., Xu, H.E., and Xu, W. (2015). Structural basis of the Norrin-Frizzled 4 interaction. Cell Res *25*, 1078-1081.
Silvie, O., Rubinstein, E., Franetich, J.F., Prenant, M., Belnoue, E., Renia, L., Hannoun, L., Eling, W., Levy, S., Boucheix, C., *et al.* (2003). Hepatocyte CD81 is required for Plasmodium falciparum and Plasmodium yoelii sporozoite infectivity. Nat Med *9*, 93-96.
Smallwood, P.M., Williams, J., Xu, Q., Leahy, D.J., and Nathans, J. (2007). Mutational analysis of Norrin-Frizzled4 recognition. J Biol Chem *282*, 4057-4068.
Starr, T.N., Greaney, A.J., Addetia, A., Hannon, W.W., Choudhary, M.C., Dingens, A.S., Li, J.Z., and Bloom, J.D. (2021). Prospective mapping of viral mutations that escape antibodies used to treat COVID-19. Science.
Stenman, J.M., Rajagopal, J., Carroll, T.J., Ishibashi, M., McMahon, J., and McMahon, A.P. (2008). Canonical Wnt signaling regulates organ-specific assembly and differentiation of CNS vasculature. Science *322*, 1247-1250.
Tan, J., Pieper, K., Piccoli, L., Abdi, A., Perez, M.F., Geiger, R., Tully, C.M., Jarrossay, D., Maina Ndungu, F., Wambua, J., *et al.* (2016). A LAIR1 insertion generates broadly reactive antibodies against malaria variant antigens. Nature *529*, 105-109.
Tan, T.K., Rijal, P., Rahikainen, R., Keeble, A.H., Schimanski, L., Hussain, S., Harvey, R., Hayes, J.W.P., Edwards, J.C., McLean, R.K., *et al.* (2021). A COVID-19 vaccine candidate using SpyCatcher multimerization of the SARS-CoV-2 spike protein receptor-binding domain induces potent neutralising antibody responses. Nat Commun *12*, 542.
Toomes, C., Bottomley, H.M., Jackson, R.M., Towns, K.V., Scott, S., Mackey, D.A., Craig, J.E., Jiang, L., Yang, Z., Trembath, R., *et al.* (2004). Mutations in LRP5 or FZD4 underlie the common familial exudative vitreoretinopathy locus on chromosome 11q. Am J Hum Genet *74*, 721-730.
Trombetta, E.S., and Parodi, A.J. (2003). Quality control and protein folding in the secretory pathway. Annu Rev Cell Dev Biol *19*, 649-676.
Umeda, R., Satouh, Y., Takemoto, M., Nakada-Nakura, Y., Liu, K., Yokoyama, T., Shirouzu, M., Iwata, S., Nomura, N., Sato, K., *et al.* (2020). Structural insights into tetraspanin CD9 function. Nat Commun *11*, 1606.
Vences-Catalan, F., and Levy, S. (2018). Immune Targeting of Tetraspanins Involved in Cell Invasion and Metastasis. Front Immunol *9*, 1277.
Walls, A.C., Park, Y.J., Tortorici, M.A., Wall, A., McGuire, A.T., and Veesler, D. (2020). Structure, Function, and Antigenicity of the SARS-CoV-2 Spike Glycoprotein. Cell *181*, 281-292 e286.
Wang, C., Li, W., Drabek, D., Okba, N.M.A., van Haperen, R., Osterhaus, A., van Kuppeveld, F.J.M., Haagmans, B.L., Grosveld, F., and Bosch, B.J. (2020a). A human monoclonal antibody blocking SARS-CoV-2 infection. Nat Commun *11*, 2251.
Wang, Q., Zhang, Y., Wu, L., Niu, S., Song, C., Zhang, Z., Lu, G., Qiao, C., Hu, Y., Yuen, K.Y., *et al.* (2020b). Structural and Functional Basis of SARS-CoV-2 Entry by Using Human ACE2. Cell *181*, 894-904 e899.
Wang, Y., Cho, C., Williams, J., Smallwood, P.M., Zhang, C., Junge, H.J., and Nathans, J. (2018). Interplay of the Norrin and Wnt7a/Wnt7b signaling systems in blood-brain barrier and blood-retina barrier development and maintenance. Proc Natl Acad Sci U S A *115*, E11827-E11836.
Watanabe, Y., Allen, J.D., Wrapp, D., McLellan, J.S., and Crispin, M. (2020). Site-specific glycan analysis of the SARS-CoV-2 spike. Science *369*, 330-333.

Weisblum, Y., Schmidt, F., Zhang, F., DaSilva, J., Poston, D., Lorenzi, J.C., Muecksch, F., Rutkowska, M., Hoffmann, H.H., Michailidis, E.*, et al.* (2020). Escape from neutralizing antibodies by SARS-CoV-2 spike protein variants. Elife *9*.

Wrapp, D., De Vlieger, D., Corbett, K.S., Torres, G.M., Wang, N., Van Breedam, W., Roose, K., van Schie, L., Team, V.-C.C.-R., Hoffmann, M.*, et al.* (2020a). Structural Basis for Potent Neutralization of Betacoronaviruses by Single-Domain Camelid Antibodies. Cell *181*, 1004-1015 e1015.

Wrapp, D., Wang, N., Corbett, K.S., Goldsmith, J.A., Hsieh, C.L., Abiona, O., Graham, B.S., and McLellan, J.S. (2020b). Cryo-EM structure of the 2019-nCoV spike in the prefusion conformation. Science *367*, 1260-1263.

Wu, Y., Li, C., Xia, S., Tian, X., Kong, Y., Wang, Z., Gu, C., Zhang, R., Tu, C., Xie, Y.*, et al.* (2020a). Identification of Human Single-Domain Antibodies against SARS-CoV-2. Cell Host Microbe *27*, 891-898 e895.

Wu, Y., Wang, F., Shen, C., Peng, W., Li, D., Zhao, C., Li, Z., Li, S., Bi, Y., Yang, Y.*, et al.* (2020b). A noncompeting pair of human neutralizing antibodies block COVID-19 virus binding to its receptor ACE2. Science *368*, 1274-1278.

Xu, Q., Wang, Y., Dabdoub, A., Smallwood, P.M., Williams, J., Woods, C., Kelley, M.W., Jiang, L., Tasman, W., Zhang, K.*, et al.* (2004). Vascular development in the retina and inner ear: control by Norrin and Frizzled-4, a high-affinity ligand-receptor pair. Cell *116*, 883-895.

Yang, J., Wang, W., Chen, Z., Lu, S., Yang, F., Bi, Z., Bao, L., Mo, F., Li, X., Huang, Y.*, et al.* (2020a). A vaccine targeting the RBD of the S protein of SARS-CoV-2 induces protective immunity. Nature *586*, 572-577.

Yang, Y., Liu, X.R., Greenberg, Z.J., Zhou, F., He, P., Fan, L., Liu, S., Shen, G., Egawa, T., Gross, M.L.*, et al.* (2020b). Open conformation of tetraspanins shapes interaction partner networks on cell membranes. EMBO J *39*, e105246.

Yao, H., Song, Y., Chen, Y., Wu, N., Xu, J., Sun, C., Zhang, J., Weng, T., Zhang, Z., Wu, Z.*, et al.* (2020). Molecular Architecture of the SARS-CoV-2 Virus. Cell *183*, 730-738 e713.

Yuan, M., Wu, N.C., Zhu, X., Lee, C.D., So, R.T.Y., Lv, H., Mok, C.K.P., and Wilson, I.A. (2020). A highly conserved cryptic epitope in the receptor binding domains of SARS-CoV-2 and SARS-CoV. Science *368*, 630-633.

Zhang, C., Lai, M.B., Pedler, M.G., Johnson, V., Adams, R.H., Petrash, J.M., Chen, Z., and Junge, H.J. (2018). Endothelial Cell-Specific Inactivation of TSPAN12 (Tetraspanin 12) Reveals Pathological Consequences of Barrier Defects in an Otherwise Intact Vasculature. Arterioscler Thromb Vasc Biol *38*, 2691-2705.

Zhou, P., Yang, X.L., Wang, X.G., Hu, B., Zhang, L., Zhang, W., Si, H.R., Zhu, Y., Li, B., Huang, C.L.*, et al.* (2020a). A pneumonia outbreak associated with a new coronavirus of probable bat origin. Nature *579*, 270-273.

Zhou, T., Tsybovsky, Y., Gorman, J., Rapp, M., Cerutti, G., Chuang, G.Y., Katsamba, P.S., Sampson, J.M., Schon, A., Bimela, J.*, et al.* (2020b). Cryo-EM Structures of SARS-CoV-2 Spike without and with ACE2 Reveal a pH-Dependent Switch to Mediate Endosomal Positioning of Receptor-Binding Domains. Cell Host Microbe *28*, 867-879 e865.

Zhu, G.Z., Miller, B.J., Boucheix, C., Rubinstein, E., Liu, C.C., Hynes, R.O., Myles, D.G., and Primakoff, P. (2002). Residues SFQ (173-175) in the large extracellular loop of CD9 are required for gamete fusion. Development *129*, 1995-2002.

Zhu, N., Zhang, D., Wang, W., Li, X., Yang, B., Song, J., Zhao, X., Huang, B., Shi, W., Lu, R., *et al.* (2020). A Novel Coronavirus from Patients with Pneumonia in China, 2019. N Engl J Med *382*, 727-733.

Zimmerman, B., Kelly, B., McMillan, B.J., Seegar, T.C.M., Dror, R.O., Kruse, A.C., and Blacklow, S.C. (2016). Crystal Structure of a Full-Length Human Tetraspanin Reveals a Cholesterol-Binding Pocket. Cell *167*, 1041-1051 e1011.

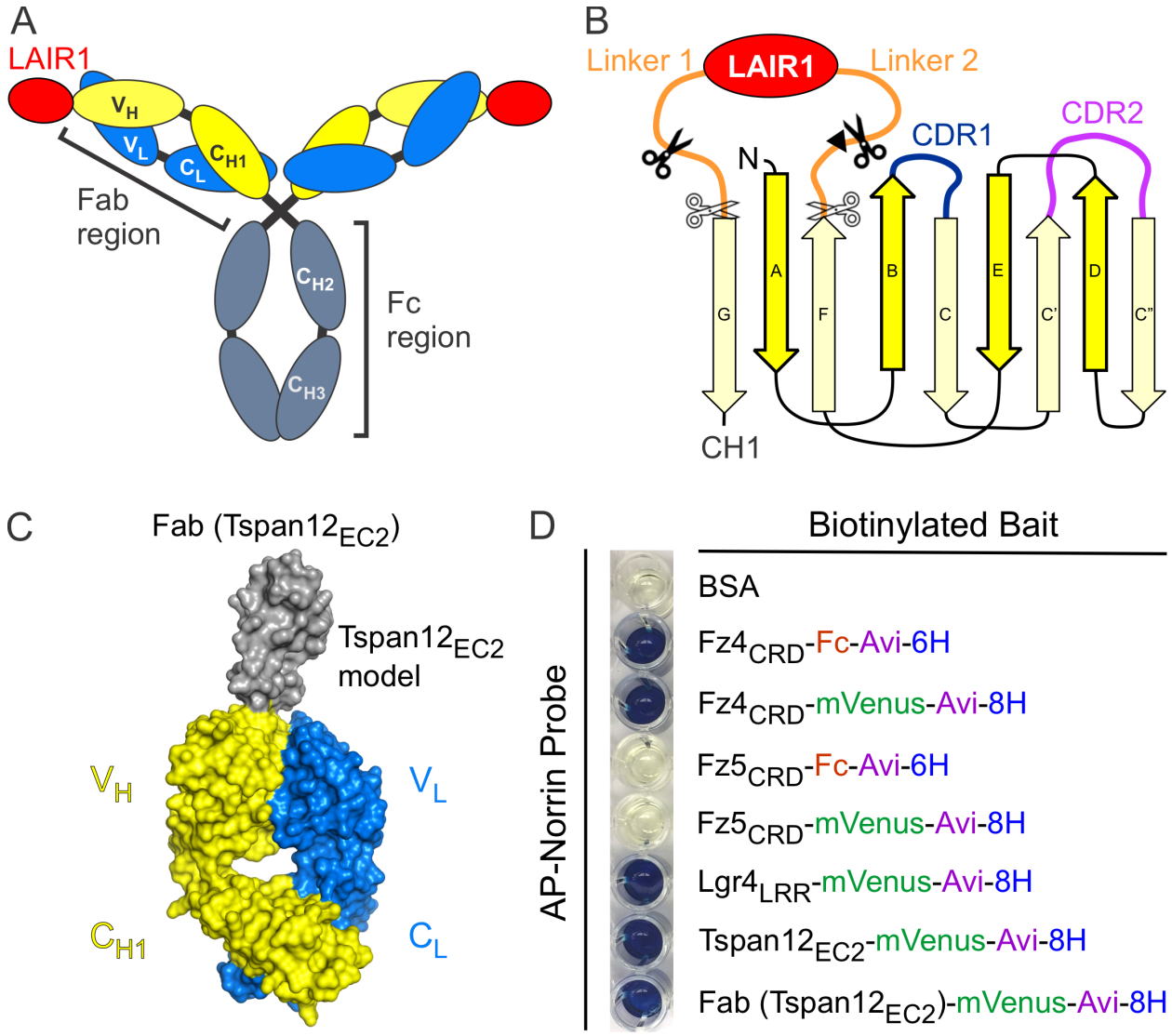

Figure 1. Antibody Display Tspan12$_{EC2}$ (Tspan12$_{EC2}$-AD). **(A)** Schematic representation of a LAIR1-containing antibody. Each Fab region is composed of variable domains of the heavy chain (V_H) and the light chain (V_L), constant domains of the heavy chain (C_{H1}) and the light chain (C_L), and a LAIRI insert on the V_H. The Fc region contains constant domains of the heavy chain (C_{H2} and C_{H3}). **(B)** Diagram representation of a LAIRI insert on the V_H and the construct design for Tspan12$_{EC2}$-AD, see also **Figure 1–Figure supplement 2**. Tspan12$_{EC2}$ replaced the LAIR1 insert (red) with two connecting linkers (orange) at different insertion sites (scissors) on the V_H (yellow). A black triangle indicates the location of C223 of the V_H forming a disulphide bond with C93 of the V_L (Notably, V_L C93A mutant was used, while the V_H construct without C223), see also **Figure 1–Figure supplement 2**. **(C)** Molecular model of Tspan12$_{EC2}$-AD showing in the Fab format. **(D)** AP based protein-protein interaction assay. AP-Norrin (probe) incubated with biotinylated baits which were immobilized on streptavidin-coated wells. After washing unbound AP probes, the bound AP probes were visualized with BluePhos phosphatase substrate solution (a colorimetric AP reaction). BSA and Fz5$_{CRD}$ fusion proteins are used as negative controls.

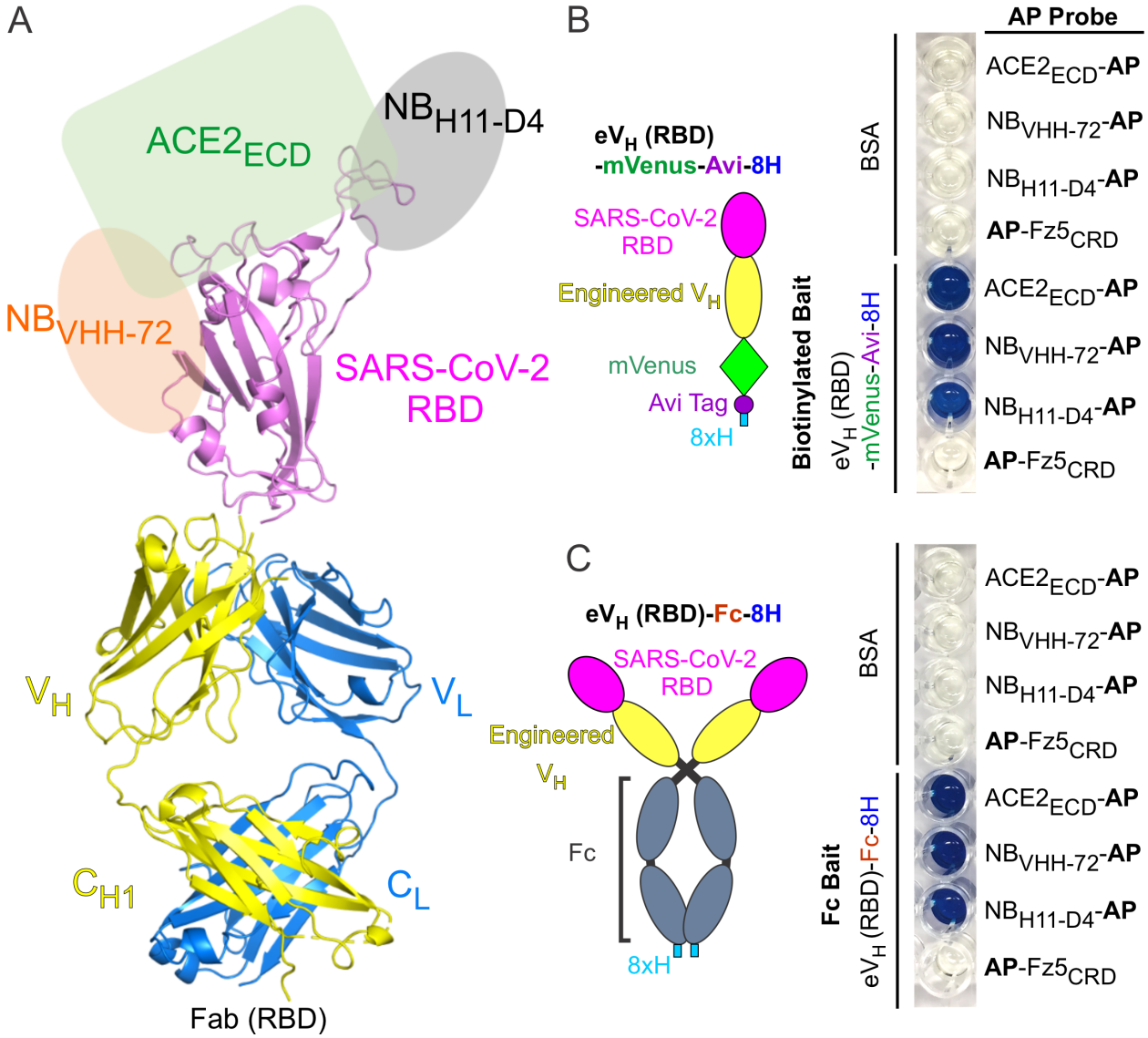

Figure 2. Antibody Display SARS-CoV-2 RBD (RBD-AD). **(A)** Molecular model of RBD-AD showing in the Fab format. The RBD (magenta) of SARS-CoV-2 S protein is displayed on the V_H (yellow). A schematic diagram shows the binding sites on the RBD for $ACE2_{ECD}$ (green), NB_{VHH-72} (orange), and NB_{H11-D4} (grey). **(B)** A diagram of the RBD of SARS-CoV-2 S protein is displayed on the engineered V_H fused to a mVenus, an Avi tag, and an 8xH tag at the C-terminus. For the AP based binding assay, biotinylated baits were immobilized on streptavidin-coated wells. Bound AP fusion proteins (probes) were visualized with BluePhos phosphatase substrate solution. BSA and $Fz5_{CRD}$ fusion proteins are used as negative controls. **(C)** Diagram of SARS-CoV-2 RBD-containing engineered V_H fused an 8xH tagged human Fc. FC baits were captured on protein-G coated wells and incubated with AP fusion proteins (probes). The bait and probe interactions were detected as in panel (B).

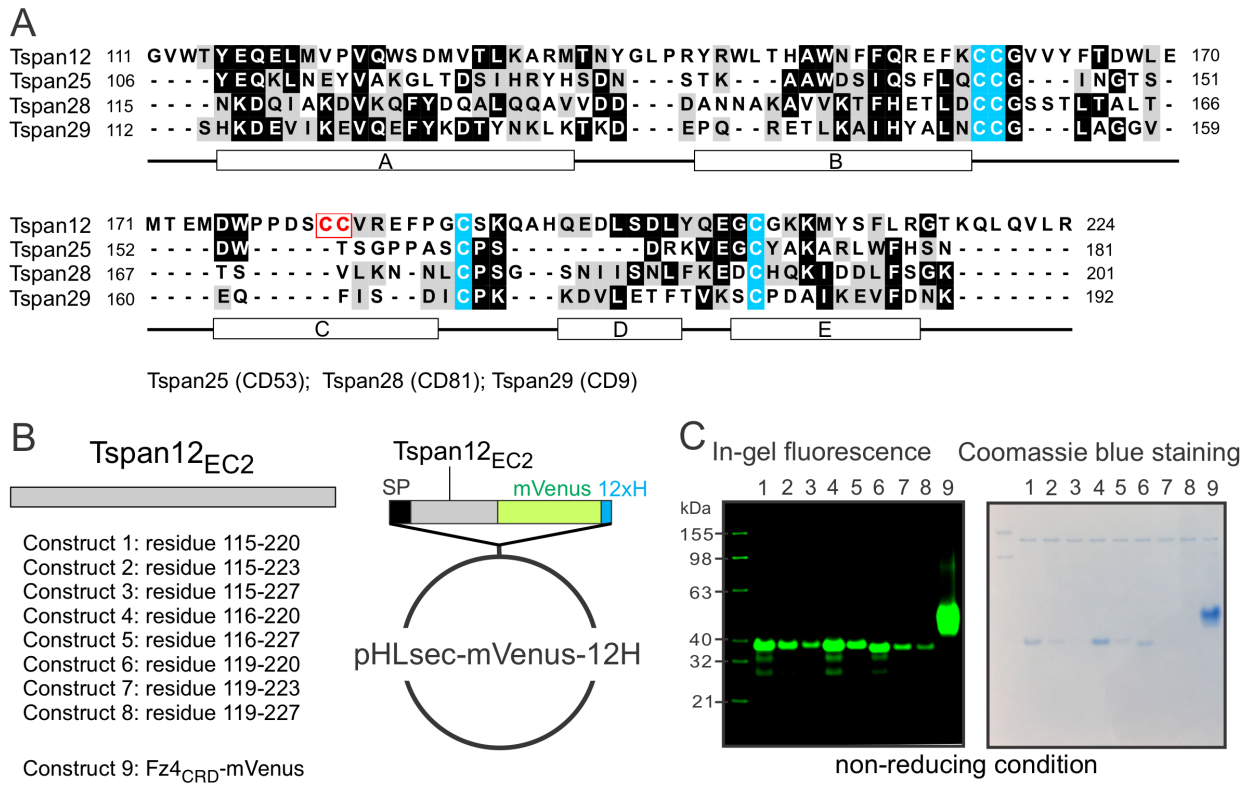

Figure 1–Figure supplement 1. Tspan12$_{EC2}$ sequence alignment, cloning, and expression trials. **(A)** Multiple sequence alignment of Tspan12$_{EC2}$ with current available Tspan structures including Tspan25 (CD53; PDB code 6WVG), Tspan28 (CD81, PDB codes 1G8Q and 5TCX), and Tspan29 (CD9, PDB codes 6RLR and 6K4J). Identical residues are shaded in dark and similar residues in grey. Secondary structure elements (five α-helical regions A to E) are indicated based on the structures of Tspan25, Tspan28, and Tspan29. The conserved cysteine residues are highlighted in cyan. Tspan12 has two additional cysteine residues (a red box) conserved in the vertebrate. **(B)** Eight Tspan12$_{EC2}$ expression constructs were cloned in the pHLsec-mVenus-12H vector. **(C)** Tspan12$_{EC2}$ constructs having the mVenus fusion were transfected in HEK293T cells. Fz4$_{CRD}$ with the mVenus fusion was used to compare the expression level. The conditioned media (1 ml) were purified by immobilized metal affinity chromatography (IMAC) and protein expression levels were determined by in-gel fluorescence imaging and Coomassie blue staining (Chang et al., 2020).

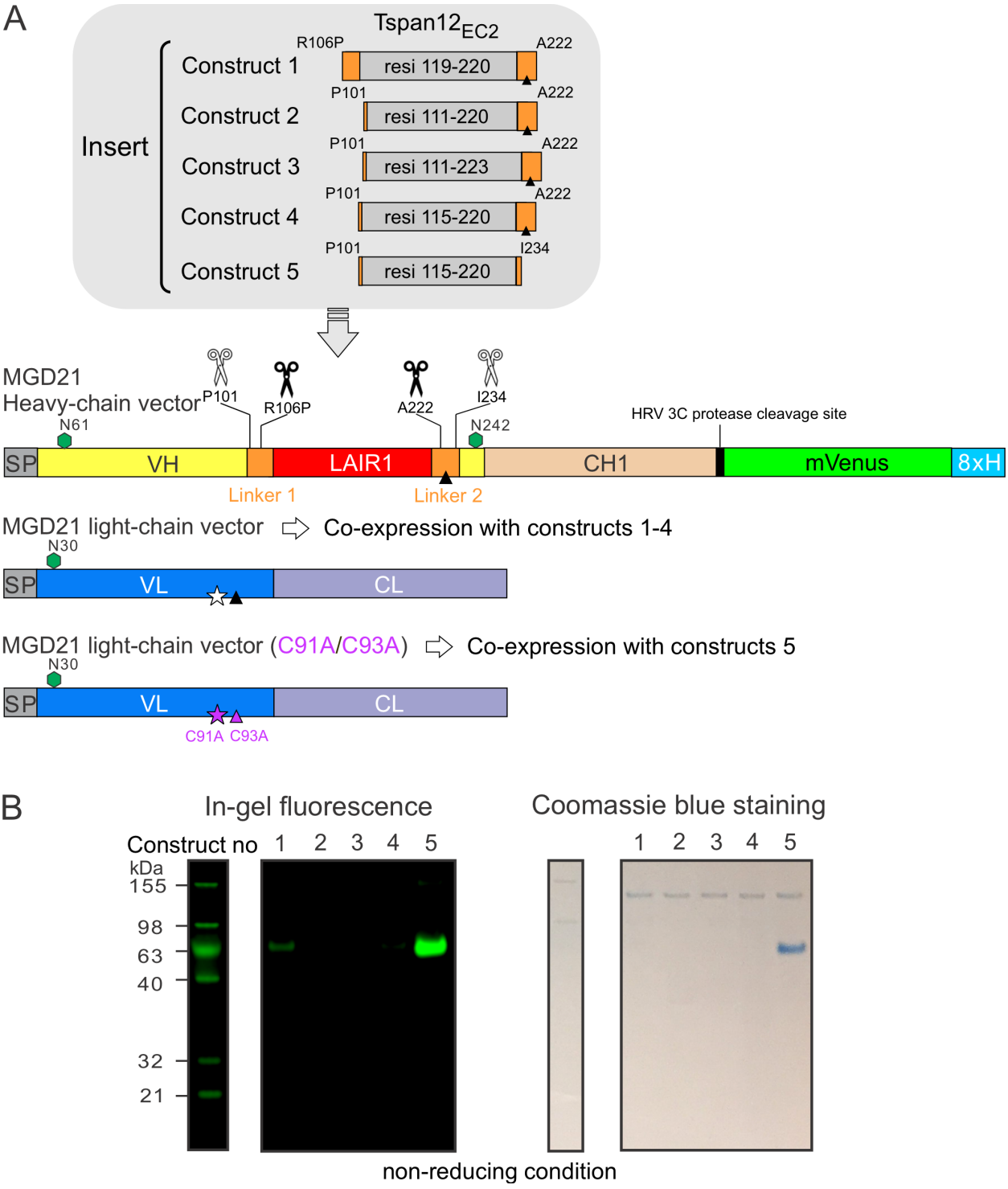

Figure 1–Figure supplement 2. Construct design and protein expression of Tspan12$_{EC2}$-AD. See also **Figure 1B** for a brief schematic representation of construct design. **(A)** Five inserts containing various fragments of Tspan12$_{EC2}$ and connecting linker sequences were cloned into a modified antibody MGD21 heavy chain vector containing a HRV 3C protease cleavage site followed by a mVenus and an 8xHis tag. Constructs 1 to 4 were co-expressed with the MGD21 light chain vector in HEK293T cells. Construct 5 which lacks residue C223 on the V_H was co-

transfected in HEK293T cells with an MGD21 light chain vector containing double mutations C91A and C93A (C93A mutation was used to block an inter-chain disulphide formation by V_H C223 and V_L C93; V_L C91 is an unpaired cysteine residue, so C91A mutation was designed to prevent the potential formation of artificial disulphide bonds). Green hexagons denote N-linked glycosylation sites. Black triangles show V_H C223. Star indicates V_L C91. **(B)** The conditioned media were harvested 2 days post-transfection and purified by IMAC. In-gel fluorescence imaging and Coomassie blue staining were used to evaluate protein expression levels.

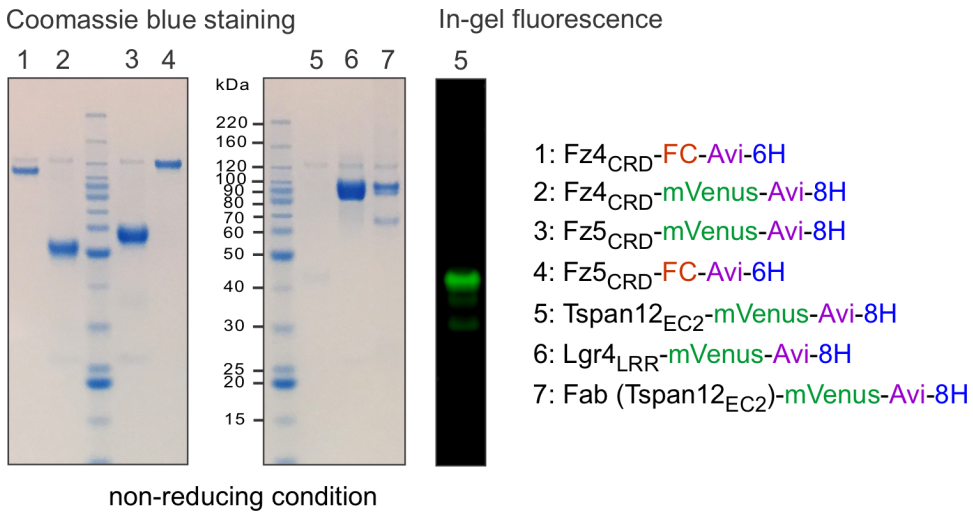

Figure 1–Figure supplement 3. Coomassie blue-stained SDS-PAGE and in-gel fluorescence imaging showed the biotinylated baits that were purified by IMAC from the conditioned media and used for the AP based binding assay (**Figure 1D**).

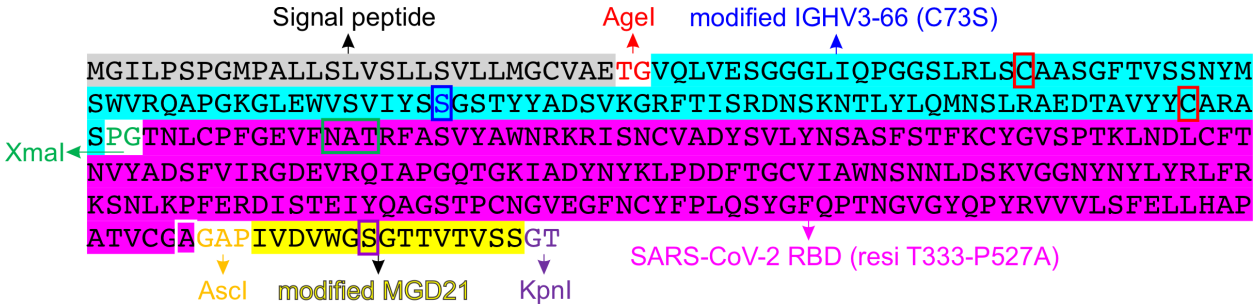

Figure 2–Figure supplement 1. The amino acid sequence of the RBD of SARS-CoV-2 S protein displayed on the engineered V_H. Engineered V_H is a chimeric fusion of the V_H region of IGHV3-66*1 highlighted in cyan (the C73S mutation is used to prevent the formation of artificial disulphide bonds and is boxed in blue) and a part of MGD21 V_H region highlighted in yellow (the N242S mutation is used to block the N-linked glycosylation and is boxed in purple; two residues, Y235 and Y236, are removed from the sequence by complementing the insertion of an AscI restriction site). The RBD (highlighted in magenta) of SARS-CoV-2 S protein contains a P527A mutation (boxed in white) by enhancing model restraint for the insertion. Red boxes denote two conserved cysteine residues of V_H forming a disulphide bond. A green box indicates an N-linked glycosylation site of the RBD of SARS-CoV-2 S protein.

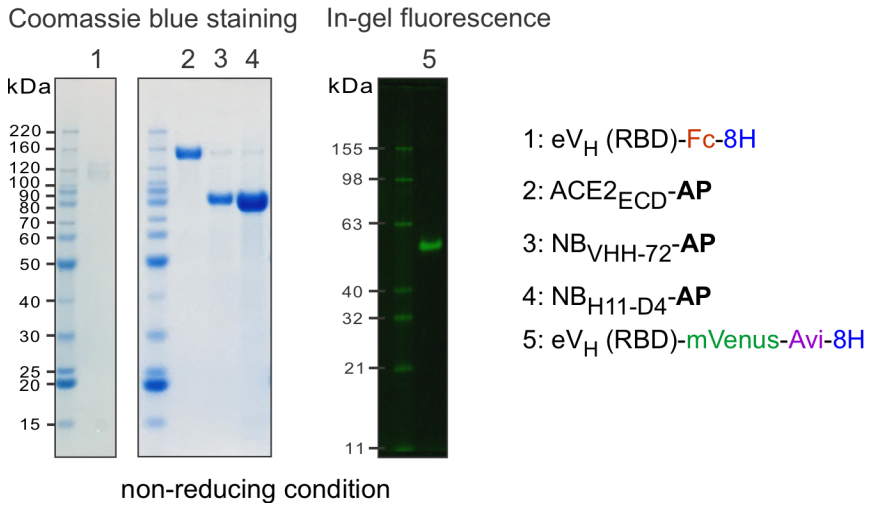

Figure 2–Figure supplement 2. Coomassie blue-stained SDS-PAGE and the in-gel fluorescence results showed the biotinylated and Fc fusion baits and AP fusion probes that were purified by IMAC from the conditioned media. Constructs of ACE2$_{ECD}$-AP, NB$_{VHH-72}$-AP, and NB$_{H11-D4}$-AP contain a C-terminal 8xHis tag. The AP based protein-protein interaction assays (**Figure 2B**, **Figure 2C** and **Figure 2–Figure supplement 3**) used the conditioned media.

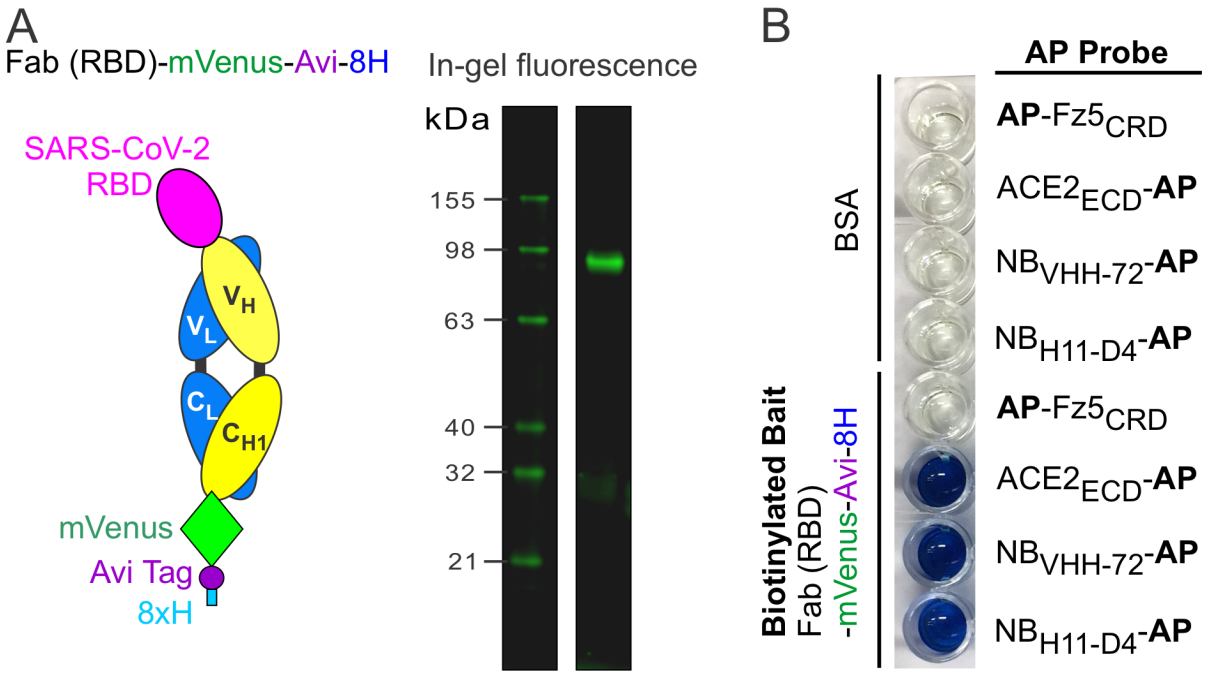

Figure 2–Figure supplement 3. Protein expression of RBD-AD in a Fab format and AP based binding assay. **(A)** The in-gel fluorescence imaging shows the biotinylated Fab (RBD)-mVenus-Avi-8H bait that was purified by IMAC from the conditioned media and used for the binding assay. **(B)** Biotinylated Fab (RBD) baits were immobilized on streptavidin-coated wells. Bound AP fusion probes were visualized by a colorimetric AP reaction (blue).